J. Am. Soc. Mass Spectrom. (2015)
DOI: 10.1007/s13361-015-1104-3

RESEARCH ARTICLE

Protonated Hexaazamacrocycles as Selective K^+ Receptors

Caterina Fraschetti,[1] Antonello Filippi,[1] Maria Elisa Crestoni,[1] Enrico Marcantoni,[2] Marco Glucini,[2] Laura Guarcini,[1] Maria Montagna,[1] Leonardo Guidoni,[3] Maurizio Speranza[1]

[1]Dipartimento di Chimica e Tecnologia del Farmaco, Università La Sapienza, Rome, Italy
[2]Scuola di Scienze e Tecnologie, Divisione Chimica, Università di Camerino, 62032, Camerino, MC, Italy
[3]Dipartimento di Scienze Fisiche e Chimiche, Università degli Studi de L'Aquila, 67100, L'Aquila, Italy

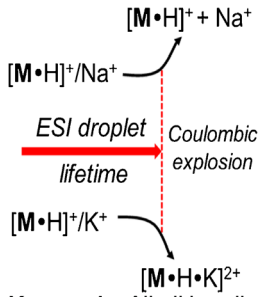

Abstract. Protonated hexaazamacrocycle $[\mathbf{M}\bullet H]^+$ is able to detect K^+ ions present at ppb level in methanolic solutions containing 10^{-5} M of Na^+ ions. The high sensitivity and selectivity of $[\mathbf{M}\bullet H]^+$ for K^+ is ascribed to the favorable energy balance between the K^+ ion desolvation and its coordination to the $[\mathbf{M}\bullet H]^+$ macrocycle, which allows the formation of the corresponding adduct before the Coulombic explosion of the ESI-MS nanodroplets.

Keywords: Alkali ion discrimination, Azamacrocyles, Desolvation effects, Dications, ESI-MS

Received: 7 January 2015/Revised: 3 February 2015/Accepted: 13 February 2015

Introduction

In recent years, the development of organic receptor molecules capable of selectively binding alkali ion has elicited wide interest in both chemical and biological fields. The exquisite selectivity and sensitivity of potassium (K^+) channels are crucial for physiological functions [1, 2]. The performance of these channels, able to select K^+ over Na^+ by a factor of 10^4, depends on the energetic balance between the alkali ion desolvation and its coordination to the peptide backbone oxygens in the narrow pore region [3–5]. Such an energy compensation has been actually taken as a guideline for developing abiotic receptors highly selective towards alkali cations. In particular, crown ethers were considered. For instance, 18-crown-6 was found to bind preferentially K^+ over the other alkali ions in aqueous solution [6, 7]. However, this behavior was not replicated in the gas phase [8–10]. Mass spectrometric [11–13] and computational [14] studies showed that ion microhydration is crucial for reconciling the solution and gas-phase selectivities.

In this frame, the discovery of a new class of abiotic receptors capable of selectively fishing trace amounts of K^+ out from other alkali cations would be desirable [15]. Interest may grow up if these receptors can work also in the gas phase under conditions, such as electrospray ionization mass spectrometry (ESI-MS), suitable for rapid-screening analyses. Recent studies showed that chiral polyazamacrocyles, like **M** (Figure 1), are able to bind efficiently metal ions [16–20] as well as carboxylic acids [21] and their conjugate bases in different solvents [22–25]. In the course of a comprehensive study on their diastereoselectivity in the gas phase, our attention was drawn by the rather unexpected observation of uncommon K^+ versus Na^+ selectivity of receptor **M** discussed in the present paper.

Experimental

Materials

Ultrapure methanol (≥99.9%), $NaNO_3$, and KNO_3 were purchased from a commercial source. The racemate of the hexaazamacrocycle M was synthesized and purified according to our modifications of the procedures reported in the literature [17, 24, 26] (see Supplementary Scheme S1). Each step of the reaction sequence was monitored by thin-layer chromatography and HPLC-ESI-mass spectrometry. Chromatographic purifications were carried out through flash-chromatography on

Electronic supplementary material The online version of this article (doi:10.1007/s13361-015-1104-3) contains supplementary material, which is available to authorized users.

Correspondence to: Maurizio Speranza; *e-mail:* maurizio.speranza@uniroma1.it

Published online: 09 April 2015

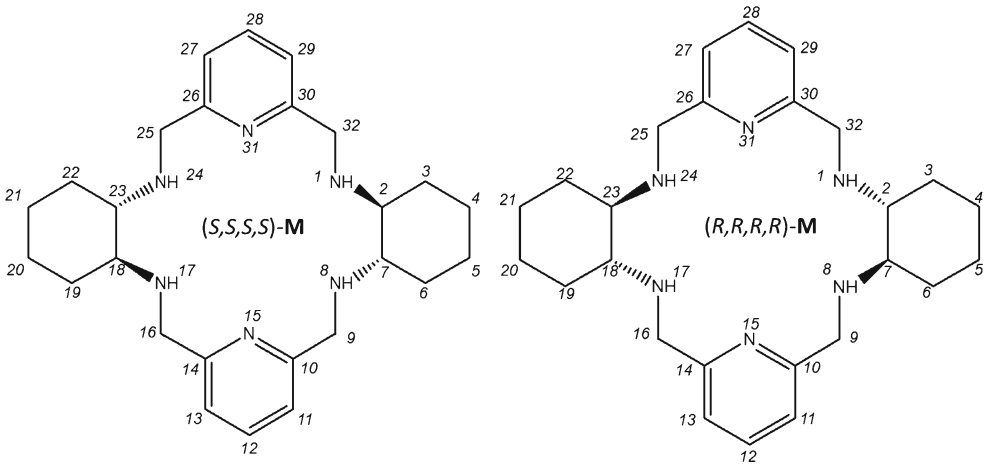

Figure 1. Chemical structure of the (*S,S,S,S*) and (*R,R,R,R*) enantiomers of the 18-membered hexaazamacrocycle **M**

Silica Gel Merck (mesh 0.040–0.063) Merck KGaA, Darmstadt, Germany. Mass spectra were obtained using an Agilent 110 MSD ion-trap mass spectrometer Agilent Technolofy, Santa Clara, CA, 95051, USA equipped with a standard ESI/APCI source. ^{1}H and ^{13}C NMR spectra were recorded in a $CDCl_3$ solution on a Varian Mercury plus 400 MR Varian Inc., Palo Alto, CA, USA (at 400 MHz and 100 MHz, respectively). Chemical shifts were quoted in ppm and were referenced to residual H in deuterated solvent as the internal standard. The elemental analyses were carried out on a Perkin-Elmer 2400 CHN elemental analyzer Perkin Elmer Inc. Palo Alto, CA, USA.

Mass Spectrometry

The ESI-MS experiments were carried out in an Applied Biosystems Linear Ion Trap (LIT) API 2000 mass spectrometer (Applied Biosystems, Foster City, CA 94404 USA) equipped with an ESI source and a syringe pump. Operating conditions of the ESI source are as follows: ion spray voltage=+5.5 kV; curtain gas=20 psi; nebulizer gas=20 psi; entrance potential=+10 V; declustering potential=+60 V; capillary temperature=150°C. Methanol and water/methanol solutions were infused via a syringe pump at a flow rate of 3 μL min^{-1}. The relative abundance of peaks results from their area acquired in profile mode. In each acquisition the final spectra are the average of about 10 scans. The $[M•K•H]^{2+}$ ions were submitted to collisional induced dissociation (collision energies employed up to 40 eV, lab frame) using N_2 gas into the trap (nominal pressure into the trap, 4.0×10^{-5} Torr). High resolving power spectra have been obtained using a Bruker BioApex Fourier transform ion cyclotron resonance (FT-ICR) mass spectrometer (Bruker, Billerica, MA,USA) equipped with an Apollo I electrospray ionization (ESI) source, a 4.7 T superconducting magnet, and a cylindrical infinity cell. Operating conditions of the ESI source were as follows: ion spray voltage=+4.0 kV; nebulizer gas (N_2)=15 psi; drying gas (N_2)=5 psi; end plate=+4.0 kV; capillary exit 100 V; dry temperature=200°C.

Computational Details

A preliminary investigation on the potential energy surfaces (PESs) of the $[\mathbf{M}•H]^+$, $[\mathbf{M}•Na]^+$, $[\mathbf{M}•K]^+$, and $[\mathbf{M}•H]^{2+}$ and ions have been carried on using classic molecular dynamics (MD) simulations based on Amber [27] force field. According to the procedure exploited by Vaden et al. [28], a simulated annealing approach was performed in order to investigate the conformational space. The minimum energy conformers found by MD have been optimized at quantum mechanics level. For optimized geometries and frequencies calculations we have used Density Functional Theory approach using B3LYP [29] exchange-correlation functional and the 6-31G* basis set. We employed the Orca [30] package with a SCF convergence criteria set as TightSCF (energy change 1e-08; max density change 1e-07; rms-density change 1e-09) and a high precision for the integration grids. Geometry optimizations were carried out without any constraint. Concerning the $[\mathbf{M}•K•H]^{2+}$ and $[\mathbf{M}•Na•H]^{2+}$ ions, because of the inadequacy of classical simulated annealing, ab initio molecular dynamics simulations (AIMD) were carried out in order to investigate the conformational space. The AIMD were carried out using Terachem package [31], and the trajectory was evolved according to the Born-Oppenheimer scheme [32]. The electronic structure of the system was treated at the DFT level of theory with the BLYP exchange-correlation functional [33] and 6-31G* basis set. Dynamic simulations were performed for 10 ps and at different temperature (500 and 700 K) controlled via a Nose-Hoover thermostat [34, 35]. Some snapshots of trajectory are extracted and optimized at B3LYP/6-31G* level of theory to sample the local conformational space.

Results and Discussion

ESI-MS analyses of methanolic solutions containing the racemate of the hexaazamacrocycle **M** (10^{-5} M) showed the presence of an intense signal at *m/z* 435, identified as $[\mathbf{M}•H]^+$, and much smaller peaks at *m/z* 457 ($[\mathbf{M}•Na]^+$) and *m/z* 473 ($[\mathbf{M}•K]^+$) (Figure 2). These species were accompanied by

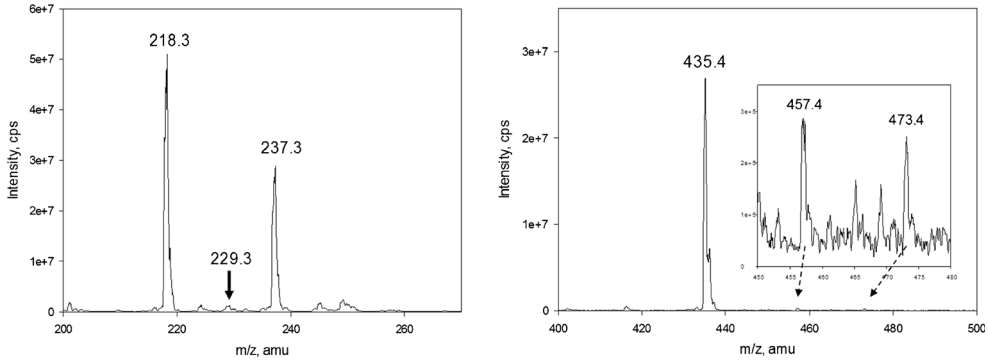

Figure 2. ESI-MS spectrum of 10–5 M methanolic solutions of **M**

intense signals corresponding to the $[\mathbf{M}\bullet H_2]^{2+}$ (*m/z* 218) and $[\mathbf{M}\bullet H\bullet K]^{2+}$ (*m/z* 237) dications. Quite unexpectedly, the $[\mathbf{M}\bullet H\bullet Na]^{2+}$ analogue (*m/z* 229) was virtually absent (see also Supplementary Figure S1). Collision induced dissociation (CID) experiments have been carried out on the $[\mathbf{M}\bullet H\bullet K]^{2+}$ dication. Even after multiple collisions [36, 37] at energies up to 40 eV (lab frame), no meaningful fragmentation was observed. It should be pointed out that the formation of $[\mathbf{M}\bullet H_2]^{2+}$, but not of $[\mathbf{M}\bullet H\bullet K]^{2+}$, was previously observed by Gotor-Fernandez et al. from ESI-MS of aqueous **M** solutions [24].

It should be stressed again that no alkali ions were purposely introduced in the **M** methanolic solutions before ESI-MS analysis. Nevertheless, in the ESI nanodroplet, protonated **M** seems to be able to bind K^+ ions 20 times more efficiently than the Na^+ one. This means that since the level of sodium ions in ultrapure methanol (≥99.9%) does not exceed 1 ppm, the azamacrocyle **M** is able to detect K^+ ions at ppb levels. With the aim of further substantiating this conclusion, several calibrated $KNO_3/NaNO_3$ methanolic solutions have been prepared and submitted to ESI-MS analyses under the same experimental conditions. The results, summarized in Figure 3, show that the $[\mathbf{M}\bullet H]^+$ and $[\mathbf{M}\bullet Na]^+$ cations predominate over the $[\mathbf{M}\bullet K]^+$ one under all conditions. The $[\mathbf{M}\bullet Na]^+/[\mathbf{M}\bullet K]^+$ ratios range from 7 to 9 and, especially at the lowest K^+ concentrations ($[K^+]=10^{-7}$–10^{-9} M), do not reflect the $[Na^+]/[K^+]$ ones. This can be attributed in part to the increased yield of the $[\mathbf{M}\bullet H_2]^{2+}$ ion to the expenses of $[\mathbf{M}\bullet Na]^+$. However, at the lowest K^+ concentration ($[K^+]=10^{-9}$ M; log($[Na^+]/[K^+]$)=4), the abundance of the $[\mathbf{M}\bullet H\bullet K]^{2+}$ ion is still ca. nine times that of $[\mathbf{M}\bullet H\bullet Na]^{2+}$ and, therefore, the azamacrocyle is able to detect K^+ ions at a concentration of 10^{-9} M or even lower in agreement with the above estimate.

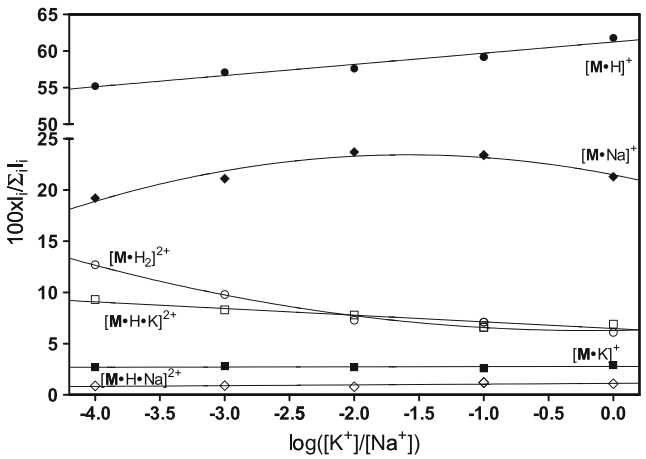

Figure 3. Percent distribution of the major ionic species observed in the ESI-MS of **M** (10^{-5} M)/KNO_3 (10^{-9}–10^{-5} M)/NaNO3 (10^{-5} M) methanolic solutions as a function of the $[K^+]/[Na^+]$ ratio

Two major reaction mechanisms can be hypothesized for formation of $[\mathbf{M}\bullet H\bullet A]^{2+}$ (A=Na, K) in the ESI nanodroplets. One involving the preliminary protonation of the **M** macrocycle followed by the addition of the alkali ion [route (a)], the other though the protonation of a preformed $[\mathbf{M}\bullet A]^+$ (A=Na, K) cation [route (b)].

Quantum mechanical calculations at B3LYP/6-31G* level of theory were employed for the description of the structure and energetics of all the ionic species of Scheme 1 and Figure 3. Six isomeric structures are available to the $[\mathbf{M}\bullet H_2]^{2+}$ dication (Supplementary Figure S4) with the $\mathbf{IV}_{1,17}$ one as the most stable at 298 K [17, 24]. Structures $\mathbf{V}_1$ (Supplementary Figure S5) and $\mathbf{VI}_1$ (Supplementary Figure S6) are the most stable isomers of $[\mathbf{M}\bullet H\bullet Na]^{2+}$ and $[\mathbf{M}\bullet H\bullet K]^{2+}$, respectively. From the corresponding 298 K free energy values, it was possible to calculate the ΔG_{298} of the processes listed in Table 1.

The ΔG_{298}=0 kJ mol^{-1}, calculated for reaction (3), indicates that the $[\mathbf{M}\bullet Na]^+$ and $[\mathbf{M}\bullet K]^+$ ions exhibit the same gas-phase basicity. This piece of information, coupled with the large $[\mathbf{M}\bullet H\bullet K]^{2+}$ vs. $[\mathbf{M}\bullet H\bullet Na]^{2+}$ imbalance, despite $[\mathbf{M}\bullet Na]^+/[\mathbf{M}\bullet K]^+ \geq 1$ (Figures 2 and 3), speaks against route (b) of Scheme 1 as a predominant mechanism of formation of the $[\mathbf{M}\bullet H\bullet K]^{2+}$ dication in the ESI nanodroplet. Rather, formation of this dication likely proceeds through route (a) of Scheme 1, namely through the addition of the alkali cation to $[\mathbf{M}\bullet H]^+$.

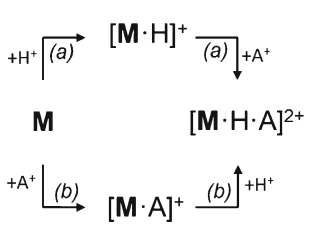

Scheme 1. Possible reaction routes to [M•H•A]2+ (A=Na, K) in the ESI-MS nanodroplets

Table 1. Reaction Free Energies

Reaction	No.	ΔG_{298} (kJ mol^{-1})
$[\mathbf{M}\bullet K]^+ + Na^+ \rightarrow [\mathbf{M}\bullet Na]^+ + K^+$	(1)	–117
$[\mathbf{M}\bullet H\bullet K]^{2+} + Na^+ \rightarrow [\mathbf{M}\bullet H\bullet Na]^{2+} + K^+$	(2)	–117
$[\mathbf{M}\bullet H\bullet K]^{2+} + [\mathbf{M}\bullet Na]^+ \rightarrow [\mathbf{M}\bullet H\bullet Na]^{2+} + [\mathbf{M}\bullet K]^+$	(3)	0

The ΔG_{298}=−117 kJ mol^{-1}, calculated for reactions (1) and (2), indicates that formation of the sodiated adducts is favored over that of the K^+-containing analogues and that, if the processes were reversible, the imbalance between these adducts would increase by increasing the $[Na]^+/[K]^+$ ratio. However, the relative constancy of the $[\mathbf{M}\bullet Na]^+/[\mathbf{M}\bullet K]^+$ and $[\mathbf{M}\bullet H\bullet Na]^{2+}/[\mathbf{M}\bullet H\bullet K]^{2+}$ ratios of Figure 3, despite a change of the $[Na]^+/[K]^+$ ratio from 1 to 10^4, strongly suggests that in the ESI nanodroplets the alkali cation addition to **M** (or to $[\mathbf{M}\bullet H]^+$) is not reversible and that equilibration between the relative adducts does not take place. Therefore, the ion pattern of Figure 3 is thought to respond to the kinetics of the process taking place in the ESI nanodroplets. Along this line, the only plausible rationale for the spectacular K^+ versus Na^+ selectivity of $[\mathbf{M}\bullet H]^+$ can be found in the corresponding activation free energy barriers reflecting the desolvation of the alkali ion while coordinating to the receptor (i.e., the same factors accounting for the exceptional K^+ over Na^+ selectivity of biotic potassium channels [3–5].

Table 2 compares the absolute 298 K free energy (ΔG_{solv}) values of Na^+ and K^+ in water and methanol, calculated using cluster continuum quasichemical theory of solvation [38, 39]. The listed values indicate that the Na^+ desolvation free energy is 73 (methanol) or 84 kJ mol^{-1} (water) larger than that of K^+. Moreover, the desolvation free energy of both ions in methanol is ca. 41–52 kJ mol^{-1} lower than in water. In the same Table, the 298 K binding free energies (ΔG_M) for the addition of alkali cations to neutral **M** are given. Comparison of the ΔG_M values with the corresponding ΔG_{solv} reveals that the alkali ion desolvation from methanol or water can be fully counterbalanced by the interaction energy with **M**.

As shown in Supplementary Figure S3, the Na^+ cation is placed inside the receptor cavity, whereas the K^+ ion resides above it and, therefore, the reorganization of the **M** structure around K^+ to yield the $[\mathbf{M}\bullet K]^+$ adduct is expected to cause a less extensive ion desolvation than that yielding $[\mathbf{M}\bullet Na]^+$. It is conceivable that the ion desolvation induced by **M** when forming the corresponding adduct may have a hand in building an activation barrier, which should be larger for the formation of $[\mathbf{M}\bullet Na]^+$ than for $[\mathbf{M}\bullet K]^+$. Accordingly, in the ESI nanodroplets, the formation of the $[\mathbf{M}\bullet K]^+$ adduct could be significantly faster than that of $[\mathbf{M}\bullet Na]^+$. Now, an important requirement for the observation of an ionic species by ESI-MS is that its formation timing must exceed the average lifetime of the ESI nanodroplet before Coulombic explosion. It is proposed that by the time of the nanodroplet explosion, the formation of the $[\mathbf{M}\bullet K]^+$ adducts is very advanced upon that of the $[\mathbf{M}\bullet Na]^+$ ones and, therefore, their relative abundance is comparable in spite of the large $[Na^+]$ versus $[K^+]$ imbalance (Figure 3).

The same concept can be extended to the competing formation of the $[\mathbf{M}\bullet H\bullet A]^{2+}$ (A=Na, K) dications. Because of charge repulsion, desolvation of the A^+ cation by $[\mathbf{M}\bullet H]^+$ in the ESI nanodroplets is expected to be more energy demanding and, therefore, much slower than that involving the neutral **M**. Nevertheless, $[\mathbf{M}\bullet H]^+$-induced desolvation of K^+ seems to be sufficiently fast to precede the Coulombic explosion of the nanodroplet, whereas the same process with Na^+ is not.

That alkali ion desolvation is crucial for the $[\mathbf{M}\bullet H\bullet K]^{2+}$ formation it is demonstrated by the plots in Figure 4, showing the dependence of the relative abundance of the $[\mathbf{M}\bullet H_2]^{2+}$, $[\mathbf{M}\bullet H\bullet Na]^{2+}$, $[\mathbf{M}\bullet H\bullet K]^{2+}$, and $[\mathbf{M}\bullet H]^+$ ions upon the addition of variable concentrations of water to methanol. According to Table 2, the alkali ion desolvation free energy is expected to increase by increasing the molar fraction of water in methanol. The consequence would be a pronounced decrease of the $[\mathbf{M}\bullet H\bullet K]^{2+}$ dication, as actually observed (Figure 4).

Table 2. Absolute Solvation Free Energies of Alkali Cations[a]

Cation	Solvent	ΔG_{solv} (kJ mol^{-1})
Na^+	Water[b]	–436
	Methanol[c]	–384
K^+	Water[b]	–352
	Methanol[c]	–311
		ΔG_M (kJ mol^{-1})
Na^+	**M** (one molecule)[d]	–487
K^+		–369

[a]Temperature of 298 K
[b]Ref. [38]
[c]Ref. [39]
[d]This work

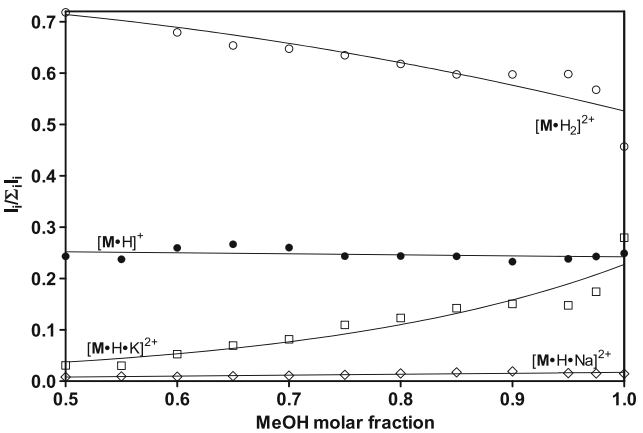

Figure 4. Solvent composition effect on the relative abundance of some ions ESI-formed from hydroalcoholic solutions containing exclusively 10^{-5} M of **M** (Figure 2)

Conclusion

The present investigation shows that the ion pattern from ESI-MS of **M** solutions is strongly dependent on the nature and the composition of the solvent employed. The protonated **M** macrocycle is able to detect K^+ ions present at ppb level in methanol. The selective formation of the $[\mathbf{M}\bullet H\bullet K]^{2+}$ ion is essentially attributed to the comparatively low free energy barrier for the structural reorganization of the protonated receptor around the desolvating K^+ ion. The extremely high sensitivity and selectivity of the $[\mathbf{M}\bullet H]^+$ ion for K^+ ions compares well with the performance of biotic K^+ channels.

Acknowledgments

The authors acknowledge support for this work by the Ministero dell'Istruzione dell'Università e della Ricerca of Italy (PRIN 2010–2011: CUP B81J1200283001, prot. 2010ERFKXL_006).

References

1. Egwolf, B., Roux, B.: Ion selectivity of the KcsA channel: a perspective from multi-ion free energy landscapes. J. Mol. Biol. **401**, 831–842 (2010)
2. Moczydlowski, E.: Chemical basis for alkali cation selectivity in potassium-channel proteins. Chem. Biol. **5**, R291–R301 (1998)
3. Zhou, Y., Morals-Cabral, J.H., Kaufman, A., MacKinnon, R.: Chemistry of ion coordination and hydration revealed by a K^+ channel-Fab complex at 2.0 Å resolution. Nature **414**, 43–48 (2001)
4. Morals-Cabral, J.H., Zhou, Y., MacKinnon, R.: Energetic optimization of ion conduction rate by the K^+ selectivity filter. Nature **414**, 37–42 (2001)
5. Dudev, T., Lim, C.: Determinants of K^+ versus Na^+ selectivity in potassium channels. J. Am. Chem. Soc. **131**, 8092–8101 (2009)
6. Izatt, R.M., Rytting, J.H., Nelson, D.P., Haymore, B.L., Christensen, J.J.: Binding of alkali metal ions by cyclic polyethers: significance in ion-transport processes. Science **164**, 443–444 (1969)
7. Christensen, J.J., Hill, J.O., Izatt, R.M.: Ion binding by synthetic macrocyclic compounds. Science **174**, 459–467 (1971)
8. Brodbelt, J.S., Liou, C.C.: New frontiers in host–guest chemistry: the gas phase. Pure Appl. Chem. **65**, 409–414 (1993)
9. Maleknia, S., Brodbelt, J.: Gas-phase selectivities of crown ethers for alkali metal ion complexation. J. Am. Chem. Soc. **114**, 4295–4298 (1992)
10. Dearden, D.V., Zhang, H., Chu, I.H., Wong, P., Chen, Q.: Macrocyclic chemistry without solvents: gas-phase reaction rates. Pure Appl. Chem. **65**, 423–428 (1993)
11. More, M.B., Ray, D., Armentrout, P.B.: Intrinsic affinities of alkali cations for 15-crown-5 and 18-crown-6: bond dissociation energies of gas-phase M^+-crown ether complexes. J. Am. Chem. Soc. **121**, 417–423 (1999)
12. Armentrout, P.B.: Cation-ether complexes in the gas phase: thermodynamic insight into molecular recognition. Int. J. Mass Spectrom. **193**, 227–240 (1999)
13. Rodriguez, J.D., Vaden, T.D., Lisy, J.M.: Infrared spectroscopy of ionophore-model systems: hydrated alkali metal ion 18-crown-6 ether complexes. J. Am. Chem. Soc. **131**, 17277–17285 (2009)
14. Feller, D.: Ab initio study of M^+:18-crown-6 microsolvation. J. Phys. Chem. A **101**, 2723–2731 (1997)
15. Ast, S., Schwarze, T., Mueller, H., Sukhanov, A., Michaelis, S., Wegener, J., Wolfbeis, O.S., Koerzdoerfer, T., Duerkop, A., Holdt, H.J.: A highly K^+-selective phenylaza-[18]crown-6-lariat-ether-based fluoroionophore and its application in the sensing of K^+ ions with an optical sensor film and in cells. Chem. Eur. J. **19**, 14911–14917 (2013)
16. Savoia, D., Gualandi, A.: Chiral perazamacrocycles. Synthesis and applications. Part 1. Curr. Org. Synth. **6**, 102–118 (2009)
17. Fitzsimmons, P.M., Jackels, S.C.: Helical hexaazamacrocyclic ligands containing pyridyl and (+ or –)-*trans*-diaminocyclohexyl groups: effect of ligand constraints upon metal ion binding. Inorg. Chim. Acta **246**, 301–310 (1996)
18. Li, F., Delgado, R., Costa, J., Drew, M.G.B., Felix, V.: Ditopic hexaazamacrocycles containing pyridine: synthesis, protonation and complexation studies. J. Chem. Soc. Dalton Trans. **1**, 82–91 (2005)
19. Li, F., Delgado, R., Felix, V.: Hexaazamacrocycle containing pyridine and its dicopper complex as receptors for dicarboxylate anions. Eur. J. Inorg. Chem. **22**, 4550–4561 (2005)
20. Gerus, A., Slepokura, K., Lisowski, J.: Anion and solvent induced chirality inversion in macrocyclic lanthanide complexes. Inorg. Chem. **52,** 12450–12460, and references therein (2013)
21. Gonzalez-Alvarez, A., Alfonso, I., Gotor-Fernandez, V.: An azamacrocyclic receptor as efficient polytopic chiral solvating agent for carboxylic acids. Tetrahedron Lett. **47**, 6397–6400 (2006)
22. Busto, E., Gonzalez-Alvarez, A., Gotor-Fernandez-Fernandez, V., Alfonso, I., Gotor-Fernandez, V.: Optically active macrocyclic hexaazapyridinophanes decorated at the periphery: synthesis and applications in the NMR enantiodiscrimination of carboxylic acids. Tetrahedron **66**, 6070–6077 (2010)
23. Gonzalez-Alvarez, A., Alfonso, I., Diaz, P., Garcia-Espana, E., Gotor-Fernandez, V.: A highly enantioselective abiotic receptor for malate dianion in aqueous solution. Chem. Commun. **11**, 1227–1229 (2006)
24. Gonzalez-Alvarez, A., Alfonso, I., Diaz, P., Garcia-Espana, E., Gotor-Fernandez-Fernandez, V., Gotor-Fernandez, V.: A simple helical macrocyclic polyazapyridinophane as a stereoselective receptor of biologically important dicarboxylates under physiological conditions. J. Org. Chem. **73**, 374–382 (2008)
25. Gospodarowicz, K., Holynska, M., Paluch, M., Lisowski, J.: Novel chiral hexaazamacrocycles for the enantiodiscrimination of carboxylic acids. Tetrahedron **68**, 9930–9935 (2012)
26. Gonzalez-Alvarez, A., Alfonso, I., Lopez-Ortiz, F., Aguirre, A., Garcia-Granda, S., Gotor-Fernandez, V.: Selective host amplification from a dynamic combinatorial library of oligoimines for the syntheses of different optically active polyazamacrocycles. Eur. J. Org. Chem. 1117-1127, (2004)
27. Case, D.A., Pearlman, D.A., Caldwell, J.W., Cheatham, T.E. III, Ross, W.S., Simmerling, C.L., Darden, T.A., Merz, K.M., Stanton, R.V., Cheng, A.L., Vincent, J.J., Crowley, M., Tsui, V., Radmer, R., Duan, Y., Pitera, J., Massova, I.G., Seibel, G.L., Singh, U.C., Weiner, P.J., Kollmann, P.A.: University of California: San Francisco.
28. Vaden, T.D., de Boer, T.S.J.A., Simons, J.P., Snoek, L.C., Suhai, S., Paizs, B.: Vibrational spectroscopy and conformational structure of protonated polyalanine peptides isolated in the gas phase. J. Phys. Chem. A **112**, 4608–4616 (2008)
29. Stephens, P.J., Devlin, F.J., Chabalowski, C.F., Frisch, M.J.: Ab initio calculation of vibrational absorption and circular dichroism spectra using density functional force fields. J. Phys. Chem. **98**, 11623–11627 (1994)
30. Neese, F.: Universität Bonn, Germany (2007)
31. Ufimtsev, I.S., Martinez, T.J.: Quantum chemistry on graphical processing units. 3. Analytical energy gradients, geometry optimization, and first principles molecular dynamics. J. Chem. Theory Comput. **5**, 2619–2628 (2009)
32. Marx, D., Hutter, J.: Ab Initio Molecular Dynamics: Basic Theory and Advanced Methods. Cambridge University Press, Cambridge (2009)
33. Lee, C., Yang, W., Parr, R.: Development of the Colle-Salvetti correlation-energy formula into a functional of the electron density. Phys. Rev. B **37**, 785–789 (1988)
34. Hoover, W.: Constant-pressure equations of motion. Phys. Rev. A **34**, 2499–2500 (1986)
35. Nose, S.: A molecular dynamics method for simulations in the canonical ensemble. Mol. Phys. **52**, 255–268 (1984)
36. Hopfgartner, G., Varesio, E., Tschäppät, V., Grivet, C., Bourgogne, E., Leuthold, L.A.: Triple quadrupole linear ion trap mass spectrometer for the analysis of small molecules and macromolecules. J. Mass Spectrom. **39**, 845–855 (2004)
37. Sleno, L., Volmer, D.A.: Ion activation methods for tandem mass spectrometry. J. Mass Spectrom. **39**, 1091–1112 (2004)
38. Roux, B., Yu, H.: Assessing the accuracy of approximate treatments of ion hydration based on primitive quasichemical theory. J. Chem. Phys. **132**, 234101/1–234101/13 (2010)
39. Pliego, J.R., Miguel, E.L.M.: Absolute single-ion solvation free energy scale in methanol determined by the lithium cluster-continuum approach. J. Phys. Chem. B **117**, 5129–5135 (2013)